Effect of Uveal Melanocytes on Choroidal Morphology in Rhesus Macaques and Humans on Enhanced-Depth Imaging Optical Coherence Tomography

Glenn Yiu,[1] Vivian S. Vuong,[1] Sharon Oltjen,[1] David Cunefare,[2] Sina Farsiu,[2] Laura Garzel,[3] Jeffrey Roberts,[3,4] and Sara M. Thomasy[5]

[1]Department of Ophthalmology and Vision Science, University of California-Davis, Sacramento, California, United States
[2]Department of Biomedical Engineering, Duke University, Durham, North Carolina, United States
[3]California National Primate Research Center, Davis, California, United States
[4]Department of Medicine and Epidemiology, University of California-Davis, School of Veterinary Medicine, Davis, California, United States
[5]Department of Surgical and Radiological Sciences, University of California-Davis, School of Veterinary Medicine, Davis, California, United States

Correspondence: Glenn Yiu, Department of Ophthalmology & Vision Science, University of California Davis Eye Center, 4860 Y Street, Suite 2400, Sacramento, CA 95817, USA; gyiu@ucdavis.edu.

Submitted: June 5, 2016
Accepted: September 11, 2016

Citation: Yiu G, Vuong VS, Oltjen S, et al. Effect of uveal melanocytes on choroidal morphology in rhesus macaques and humans on enhanced-depth imaging optical coherence tomography. *Invest Ophthalmol Vis Sci*. 2016;57:5764–5771. DOI: 10.1167/iovs.16-20070

Purpose. To compare cross-sectional choroidal morphology in rhesus macaque and human eyes using enhanced-depth imaging optical coherence tomography (EDI-OCT) and histologic analysis.

Methods. Enhanced-depth imaging–OCT images from 25 rhesus macaque and 30 human eyes were evaluated for choriocapillaris and choroidal–scleral junction (CSJ) visibility in the central macula based on OCT reflectivity profiles, and compared with age-matched histologic sections. Semiautomated segmentation of the choriocapillaris and CSJ was used to measure choriocapillary and choroidal thickness, respectively. Multivariate regression was performed to determine the association of age, refractive error, and race with choriocapillaris and CSJ visibility.

Results. Rhesus macaques exhibit a distinct hyporeflective choriocapillaris layer on EDI-OCT, while the CSJ cannot be visualized. In contrast, humans show variable reflectivities of the choriocapillaris, with a distinct CSJ seen in many subjects. Histologic sections demonstrate large, darkly pigmented melanocytes that are densely distributed in the macaque choroid, while melanocytes in humans are smaller, less pigmented, and variably distributed. Optical coherence tomography reflectivity patterns of the choroid appear to correspond to the density, size, and pigmentation of choroidal melanocytes. Mean choriocapillary thickness was similar between the two species (19.3 $\pm$ 3.4 vs. 19.8 $\pm$ 3.4 μm, $P = 0.615$), but choroidal thickness may be lower in macaques than in humans (191.2 $\pm$ 43.0 vs. 266.8 $\pm$ 78.0 μm, $P < 0.001$). Racial differences in uveal pigmentation also appear to affect the visibility of the choriocapillaris and CSJ on EDI-OCT.

Conclusions. Pigmented uveal melanocytes affect choroidal morphology on EDI-OCT in rhesus macaque and human eyes. Racial differences in pigmentation may affect choriocapillaris and CSJ visibility, and may influence the accuracy of choroidal thickness measurements.

Keywords: choroid, melanocytes, rhesus macaques, OCT, imaging

The choroid of the eye is a highly vascularized structure that supplies the outer retina. Histologically, it consists of a thin choriocapillaris layer that is adjacent to the retinal pigment epithelium (RPE) and Bruch's membrane, medium- and large-caliber vessels (known as Sattler's and Haller's layers, respectively), and a suprachoroidal layer, all embedded within a collagenous and elastic stroma along with melanocytes, fibroblasts, and resident immune cells.[1] The advent of enhanced-depth imaging optical coherence tomography (EDI-OCT) has revolutionized the in vivo visualization of the choroid in the clinical setting, using existing spectral-domain OCT devices and a more posterior zero-delay line to attain a greater depth of field.[2] Enhanced-depth imaging–OCT provides improved delineation of the choroidal–scleral junction (CSJ) and the ability to measure choroidal thickness in various retinal conditions.[3–5] For example, choroidal thinning can be seen in high myopia[6] and age-related choroidal atrophy,[7] while choroidal thickening may be a hallmark of central serous chorioretinopathy[8,9] and uveitic conditions such as Vogt-Koyanagi-Harada syndrome.[10–12] Loss of the choriocapillaris may also occur as a consequence of ischemia in diabetic patients,[13] and in areas of geographic atrophy in age-related macular degeneration (AMD).[14] Yet the cross-sectional visualization of choroidal morphology on EDI-OCT can be limited in some individuals, with a poorly delineated choriocapillaris layer or ill-defined CSJ.

We have recently employed OCT to survey adult middle-age and geriatric rhesus macaques at the California National Primate

Research Center (CNPRC), with the hope of characterizing age-related macular lesions that are unique to primates. Unlike rodents, which are poor models of age-related macular diseases like AMD due to their short life span and lack of a macula, nonhuman primates have ocular dimensions and retinal anatomy that are similar to those of humans, and possess a macula that may exhibit drusenoid lesions comparable to those in human disease.[15,16] While OCT imaging of the retinal layers in macaque eyes shows marked resemblance to human retina, we noted a very different appearance of the choroid in nonhuman primates. The choroid in macaques has a clearly delineated, hyporeflective choriocapillaris layer and significant signal attenuation in the posterior choroid resulting in poor visualization of the CSJ on EDI-OCT. To better understand this distinct appearance, we analyzed the choroidal reflectivity profiles of EDI-OCT images from adult rhesus macaques with age-matched human subjects, and compared these with histologic sections of macaque and human choroid. We found that cross-sectional visualization of choroidal structures including the choriocapillaris and CSJ is affected by the density, size, and pigmentation of uveal melanocytes in the choroid, and that racial differences in pigmentation in humans may affect choroidal morphology on EDI-OCT.

Methods

Subject and Eye Selection

Research on rhesus macaques (*Macaca mulatta*) followed the guidelines of the ARVO Statement for the Use of Animals in Ophthalmic and Vision Research, complied with the National Institutes of Health (NIH) Guide for the Care and Use of Laboratory Animals, and were approved by the University of California-Davis Institutional Animal Care and Use Committee. The CNPRC is accredited by the Association for the Accreditation and Assessment of Laboratory Animal Care (AAALAC) International. Adult animals were selected from the rhesus macaque colony at CNPRC that were undergoing routine semiannual physical examinations. The animals were sedated with intramuscular injection of ketamine hydrochloride, midazolam, and dexmedetomidine, followed by pupillary dilation with tropicamide. All subjects underwent complete ophthalmic examination including slit-lamp biomicroscopy, dilated fundus biomicroscopy, streak retinoscopy, A-scan biometry, and rebound tonometry, as well as spectral-domain OCT (SD-OCT) of the macula in EDI mode. Animal eyes that showed any retinal or choroidal lesions on exam, or demonstrated refractive error greater than –6 diopters (D) spherical equivalent based on streak retinoscopy, were excluded from this study.

Research in humans was approved by the Institutional Review Board of the University of California-Davis and was performed in accordance with the tenets of the Declaration of Helsinki. Age-matched human subjects were selected retrospectively from a database search of patients seen in the Vitreoretinal Service at the University of California-Davis Eye Center who had a normal ophthalmologic examination and underwent EDI-OCT macular imaging. These subjects underwent imaging for eyes that were evaluated for possible ocular pathology but in which no abnormalities were found ($n = 9$); or were contralateral eyes in patients with unilateral pathologies, such as epiretinal membrane or vitreomacular traction ($n = 7$), retinal tear or retinal detachment ($n = 6$), posterior vitreous detachment ($n = 5$), choroidal nevus ($n = 1$), white without pressure ($n = 1$), or open globe injury ($n = 1$). Eyes that had any retinal or choroidal diseases, history of vitreoretinal surgery, or myopia greater than –6 D were excluded. Effort was made to age-match human subjects to rhesus macaques (approximately 3 human years for every year in macaques), and to select a similar proportion of patients who identified themselves as white or black race.

For both rhesus macaques and humans, only one eye from each subject was selected for analysis. If both eyes qualified based on inclusion and exclusion criteria, the right eye was selected for patients with an even-numbered birth month, and the left eye selected for an odd-numbered birth month. Demographic data, including age and sex, were collected for all subjects. For macaques, cycloplegic refraction (D), intraocular pressure (mm Hg) measured by rebound tonometry, and axial length (mm) on A-scan biometry were also recorded. For human subjects, race, lens status (phakic, pseudophakic, or aphakic), best-corrected visual acuity (BCVA; logMAR), manifest refraction (D), and intraocular pressure (mm Hg) measured by applanation tonometry were collected.

Enhanced-Depth Imaging OCT

Enhanced-depth imaging–OCT imaging for both humans and rhesus macaques was performed using the Spectralis SD-OCT device (Heidelberg Engineering, Heidelberg, Germany). Enhanced-depth imaging–OCT was performed using a single 30° horizontal line scan with 1536 A-scans per B-scan, centered on the fovea, in high-resolution EDI mode. Up to 100 scans (range, 50–100) were averaged for each B-scan, using the Heidelberg eye tracking Automatic Real-Time (ART) software.

All imaging on rhesus macaques ($n = 25$) was performed by the first author (GY) at CNPRC. For nonhuman primate imaging, the head and chin rests of the imaging device were removed and replaced with a custom metal bar to allow the animal's head to rest comfortably. Animals were monitored by a trained technician and a CNPRC veterinarian (LG) at all times. The mean age of the animals was 20.3 ± 5.9 years (range, 10–30 years), with 14 females and 11 male primates. Study eyes included 14 right eyes (56%) and 11 left eyes (44%). Mean cycloplegic refraction was +0.3 ± 2.0 D spherical equivalent, mean intraocular pressure was 18.0 ± 4.1 mm Hg, and mean axial length was 19.7 ± 1.4 mm.

For humans ($n = 30$), EDI-OCT was performed by trained ophthalmic photographers at the UC Davis Eye Center. The mean age of the subjects was 62.8 ± 17.3 (range, 31–88 years), with 15 males and 15 female subjects. Eighteen were self-reported as white or Caucasian, while 12 were black or African American. Of the study eyes, 17 were right eyes (56.7%) and 13 were left eyes (43.3%); 27 were phakic (90%), and the remainder were pseudophakic. Mean logMAR BCVA was 0.11 ± 0.13 (Snellen equivalent 20/25.8), mean refractive error was +0.19 ± 2.0 D, and mean intraocular pressure was 15.1 ± 3.4 mm Hg.

OCT Image Analysis

Images were exported from Heidelberg Explorer software (version 1.8.6.0, Heidelberg Engineering) to ImageJ software (version 1.49v; http://imagej.nih.gov/ij/; provided in the public domain by the National Institutes of Health, Bethesda, MD, USA) to generate vertical reflectivity profiles at the foveal center. For each eye, reflectivity values were averaged over 10 adjacent A-scans, centered at the fovea, and presented on a scale from 0 to 1.00 grayscale units after normalization to the peak of the hyperreflective band corresponding to the RPE/Bruch's membrane, which was assigned to a value of 1.0. Reflectivity profiles from different eyes were aligned along the posterior border of this hyperreflective RPE/Bruch's membrane band for averaging.

Investigative Ophthalmology & Visual Science

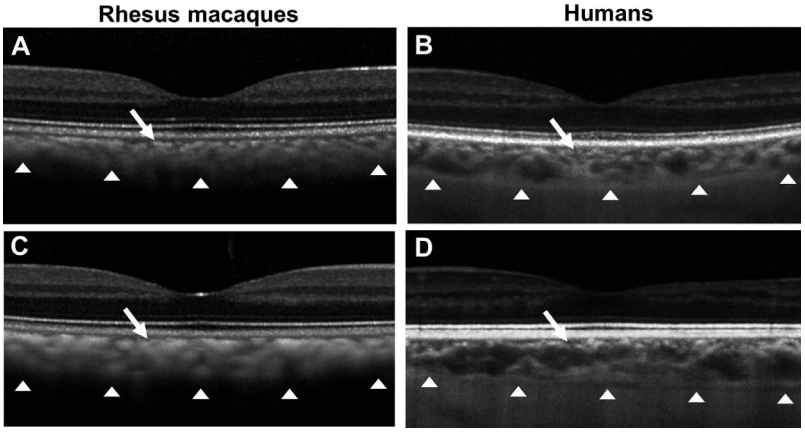

FIGURE 1. Comparison of representative EDI-OCT images from normal rhesus macaque eyes (**A**, **C**) and human eyes (**B**, **D**). The choriocapillaris layer (*arrows*) is well demarcated in rhesus macaques, but not human eyes, while the choroidal–scleral junction (*arrowheads*) is better delineated in some human eyes (33%) in comparison to macaques.

Visualization of the choriocapillaris layer and the CSJ was qualitatively graded as percent of the linear distance over which the layer boundaries were visible, and classified as clear (≥75% visibility), intermediate (≥25% and <75% visibility), or unclear (<25% visibility) by two experienced graders (GY and VV) who were masked to species and subject demographic. Any discrepancies in visibility grading were resolved by open adjudication. Choriocapillary and choroidal thicknesses were measured after semiautomated segmentation of the central 3 mm of the macula (1.5 mm nasal–1.5 mm temporal to the fovea) using Duke Optical Coherence Tomography Retinal Analysis Program (DOCTRAP, version 62.0; Durham, NC, USA), a custom image segmentation software designed using MATLAB (Mathworks, Natick, MA, USA).[17] For thickness measurements, the inner boundary was automatically determined by DOCTRAP as the outer border of the hyperreflective RPE/Bruch's complex; and two masked graders manually traced the outer border of the hyporeflective choriocapillaris layer to measure the choriocapillary thickness, and the outer border of the choroid stroma, corresponding to the CSJ, to measure the choroidal thickness.[18] All thickness measurements were determined from the mean of the two graders' measurements, and reproducibility was determined by measuring intergrader reliability using intraclass correlations (ICC) by the Bland-Altman method.[19]

Histologic Analysis

Histologic sections from rhesus macaque eyes ($n = 6$, mean age 19.2 ± 7.9 years) were taken from age-matched animals at CNPRC undergoing necropsy for nonocular health issues. Eyes were fixed in 2% paraformaldehyde and 0.5% glutaraldehyde for 24 to 48 hours, transferred to 4% formalin, then embedded in paraffin and stained with standard hematoxylin-eosin. Histologic sections from age-matched adult postmortem human eyes ($n = 10$, mean age 52.8 ± 23.5 years) were selected from an archive of cadaveric eyes with no known ocular diseases at the Duke University Medical Center (courtesy of Allan Proia). All sections also underwent standard fixation in formalin, paraffin embedding, and staining with hematoxylin-eosin. Among the eyes analyzed, five were from white subjects (mean age 63.2 ± 18.9 years, range, 35–71 years, three males/two females), and five were from black subjects (mean age 42.4 ± 24.7 years, range, 25–83 years, three males/two females).

To quantify the cell density, size, and pigmentation of choroidal melanocytes in histologic sections, three 100 × 100-μm representative regions of choroid stroma were selected for each study eye from images of histologic sections captured at ×20 using an Eclipse TE 200 (Nikon, Tokyo, Japan) microscope. We then performed automated color-based segmentation using the LAB color space and K-means clustering in MATLAB (Mathworks) to isolate the pigmented melanocytes. The number of pigmented cells in each field was manually counted to determine melanocyte density (cells per 10,000 μm^2). Average melanocyte size was calculated by dividing the total segmented area of melanin pigment by the cell number in each field. Finally, uveal pigmentation was evaluated by measuring the average luminosity (L-component of the LAB color space) of the segmented areas from each image as an estimate of optical density (Supplementary Fig. S1).

Statistical Analysis

The relationship of choriocapillaris or CSJ visibility to species or race was determined using the Kruskal-Wallis test. Multivariate ordinal logistic regression was used to determine the independent association of age, race, and refractive error with choriocapillaris or CSJ visibility. Choriocapillary and choroidal thickness measurements, as well as differences in cell density, size, and pigmentation of melanocytes, were compared using Student's *t*-tests. All statistical analyses were performed using SPSS Statistics (version 22; IBM, Armonk, NY, USA).

RESULTS

Qualitative Comparison of Choroidal Morphology on EDI-OCT

Enhanced-depth–OCT images of rhesus macaque and human eyes showed similar appearance of the retinal layers at the foveal region. However, the appearance of the choroid dramatically differed between the two species. Rhesus macaque eyes uniformly showed a distinct hyporeflective choriocapillaris layer immediately posterior to the RPE/Bruch's complex, and no distinct CSJ was seen in any of the animals (Figs. 1A, 1C). By contrast, images of human eyes showed variable appearance of the choriocapillaris, and many showed a well-delineated CSJ (Figs. 1B, 1D). Some individuals also showed a hyporeflective suprachoroidal layer as previously described (Fig. 1D).[20] Masked grading of EDI-OCT images confirmed these findings. All macaques showed ≥75% visibility

Table 1. Visibility of Choroidal Morphology in Rhesus Macaques and Humans

	Choriocapillaris Visibility			Choroidal–Scleral Junction Visibility		
Visibility	Macaques, $n = 25$	Humans, $n = 30$	P Value	Macaques, $n = 25$	Humans, $n = 30$	P Value
<25%	0, 0%	13, 43%	<0.001*	20, 80%	15, 50%	0.003*
≥25–<75%	0, 0%	10, 33%		4, 16%	5, 17%	
≥75%	25, 100%	7, 24%		1, 4%	10, 33%	

* Statistical significance ($P < 0.05$) based on Kruskal-Wallis test.

of the choriocapillaris, unlike humans, where few normal eyes showed ≥75% visibility of this layer ($P < 0.001$) (Table 1). In contrast, few macaques showed ≥25% visibility of the CSJ, while half of human subjects showed ≥25% visibility of this boundary ($P = 0.003$) (Table 1). These results show that choroidal morphology on EDI-OCT is different between rhesus macaques and humans, with better visualization of the choriocapillaris in macaques and greater visualization of the CSJ in humans.

Comparison of Reflectivity Profiles and Histology

To further compare the differential appearance of the choroidal layers in humans and macaques on EDI-OCT, we obtained vertical reflectivity profiles of the choroid at the fovea from all the images. All rhesus macaque eyes showed a narrow band of hyporeflectivity just posterior to the peak intensity of the RPE band, and delineated posteriorly by another peak of reflectivity that gradually tapers toward the sclera with no clearly demarcated vessel lumen or CSJ (Fig. 2A). Compared with histologic sections of age-matched animals, the hyporeflective band corresponds well with the location of the choriocapillaris. The signal sensitivity roll-off posterior to the choriocapillaris corresponds to the presence of large, darkly pigmented uveal melanocytes that are densely distributed between the medium- to large-caliber vessels, but not in the choriocapillaris layer. This heavy melanin pigmentation appears to result in obscuration of the CSJ in the macaque choroid.

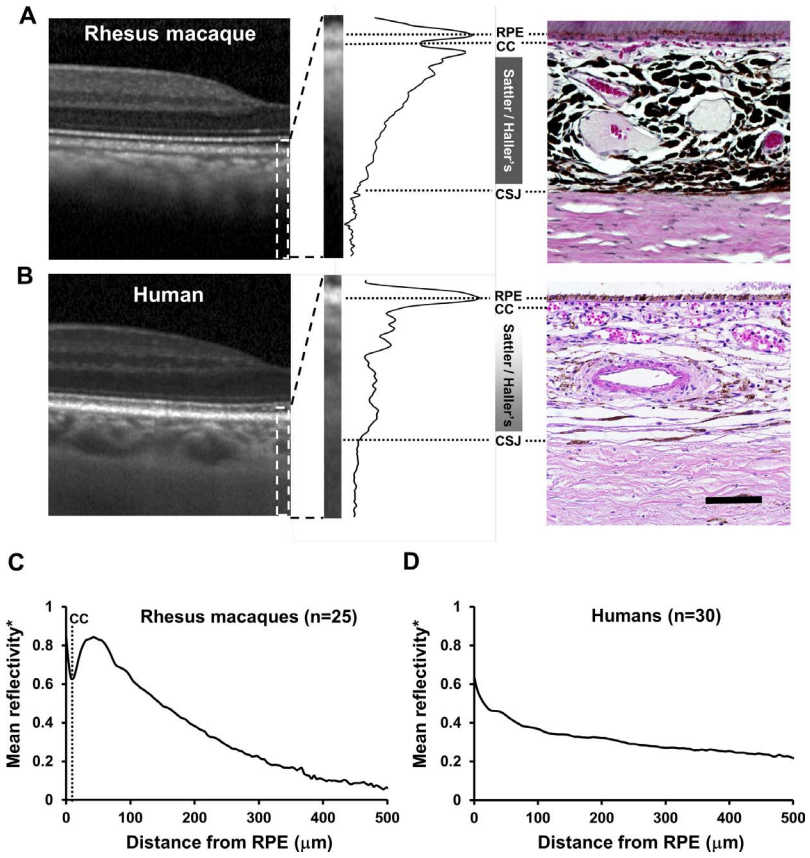

Figure 2. Reflectivity profiles of representative EDI-OCT images of a rhesus macaque (**A**) and human eye (**B**), measured from 10 adjacent A-scans centered at the fovea (magnified from area of *dashed box*). In macaques, a hyperreflective band corresponds to the RPE layer, while the adjacent hyporeflective band corresponds to the choriocapillaris (CC) on age-matched histologic sections. The gradual signal attenuation corresponds to large, darkly pigmented melanocytes that are densely distributed across the choroid stroma up to the posterior border of the choriocapillaris, and the choroidal–scleral junction (CSJ) is poorly demarcated. In humans, no distinct choriocapillaris band can be seen posterior to the hyperreflective RPE band, and the variable reflectivities of the choroidal vessels correspond to the small, lightly pigmented melanocytes that are loosely distributed mostly in the posterior choroid and suprachoroidal layer. The choroidal–scleral junction is more clearly demarcated in this white human subject. Plots of mean reflectivities of rhesus macaques (**C**) and human subjects (**D**) measured from the posterior border of the RPE/Bruch's complex, which shows a clear inflection point corresponding to the choriocapillaris in macaques but not humans. *Scale bar*: 200 μm. *Mean reflectivities are measured in arbitrary grayscale units scaled from 0 to 1.00, normalized to the peak of the RPE/Bruch's membrane, which is assigned to a value of 1.00.

Table 2. Characteristics of Choroidal Melanocytes in Rhesus Macaques and Humans

Property	Macaques, $n = 25$	Humans, $n = 30$	P Value
Cell density, cells/10K μm²	70.3 ± 8.7	34.2 ± 13.0	<0.001*
Average size, μm²/cell	72.5 ± 8.7	28.5 ± 15.8	<0.001*
Pigmentation, image luminosity	17.1 ± 4.9	96.0 ± 33.9	<0.001*

* Statistical significance ($P < 0.05$) based on Student's t-test.

By contrast, human eyes showed variable reflectivity levels between the RPE and sclera with no single distinct hyporeflective choriocapillaris, with some eyes (33%) showing a well-delineated reflectivity drop at the choroidal–scleral interface (Fig. 2B). Histologic sections of age-matched human choroid can be clearly distinguished from rhesus macaques by the smaller size and lighter pigmentation of the melanocytes (Table 2). The melanocytes are also less densely distributed and are distributed more posteriorly within the choroid stroma and in the suprachoroidal layer (Fig. 2B; Table 2). The marked difference in melanocyte pigmentation is in contrast to the RPE pigmentation, which is similar between the two species (Figs. 2A, 2B). Hence, melanin pigmentation in uveal melanocytes rather than RPE cells appears to contribute to the differential visualization of the choriocapillaris and CSJ in human and macaque eyes on EDI-OCT.

We averaged the choroidal reflectivity profiles from EDI-OCT images across all macaque animals ($n = 25$) and from all human subjects ($n = 30$) to compare differences in reflectivity patterns, and found that only the nonhuman primates exhibit a consistent clear hyporeflective band corresponding to the choriocapillaris (Figs. 2C, 2D). The mean location of the hyporeflective band is 12.5 ± 6.7 μm posterior to the posterior border of the RPE/Bruch's complex, which corresponds to the location of the choriocapillaris on histology.

Choriocapillary and Choroidal Thicknesses

Using a semiautomated graph–based OCT image segmentation software previously described,[17] we measured the thickness of the choriocapillaris and choroid along the central 3-mm segment around the fovea. The mean choriocapillary thickness was similar between rhesus macaques and humans (19.3 ± 3.4 vs. 19.8 ± 3.4 μm), with no significant difference between the two species ($P = 0.615$). However, the mean choroidal thickness measured was significantly lower in macaques compared with humans (191.2 ± 43.0 vs. 266.8 ± 78.0 μm; $P < 0.001$). In both species, while the choriocapillary thickness remains relatively constant across the central macula, the choroid is thickest at the fovea and slightly thinner in the nasal macula region (Fig. 3).

The overall intergrader reliability of choroidal thickness (ICC = 0.760) and choriocapillary thickness (ICC = 0.607) measurements was good. Consistent with the difference in choroidal morphology on EDI-OCT between the two species, the reliability of choriocapillary thickness measurements was greater than that of choroidal thickness measurements in macaque eyes (ICC = 0.661 vs. 0.297), while the opposite was true in human eyes, where measurements of choroidal thickness were more reproducible than choriocapillary thickness (ICC = 0.776 vs. 0.590). The lower reliability of choroidal thickness measurements in macaques is likely due to the poor visualization of the CSJ, and likely contributes to an underestimate of the actual choroidal thickness in these animals.

Effect of Race on Choroidal Morphology

Given the differential OCT appearance of the choroid between humans and macaques, which appears to be attributed to the marked difference in the distribution and pigmentation of choroidal melanocytes, we decided to assess whether differences in race may affect uveal pigmentation on histology and choroidal morphology on EDI-OCT. While the distribution and pigmentation of melanocytes were variable among different individuals, eyes from white subjects (Figs. 4A–C) have smaller and less darkly pigmented melanocytes than those from black individuals (Figs. 4D–F) (Table 3), as reported in prior studies.[21] Otherwise, in all human eyes, uveal melanocytes were not only smaller and less pigmented than those in rhesus macaques (Table 2), but also less densely packed and more

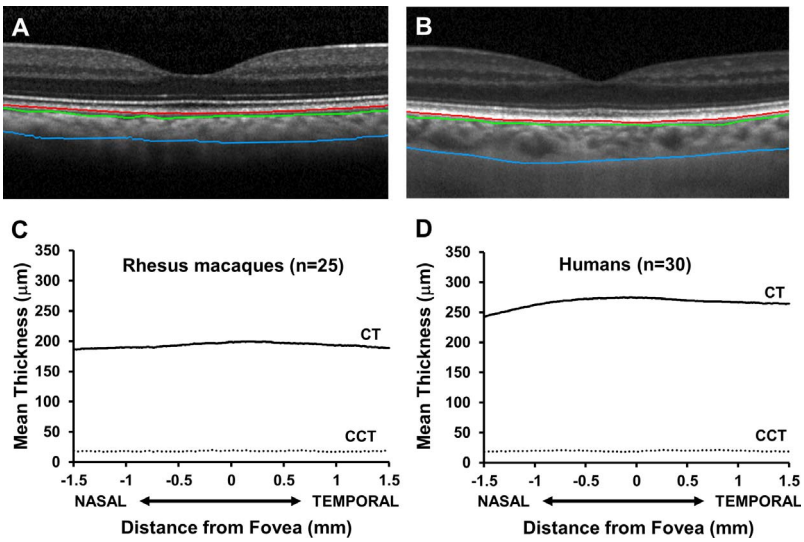

Figure 3. Representative EDI-OCT images with semiautomatic segmentation of the choriocapillaris and choroid stroma in rhesus macaque (**A**) and human eyes (**B**). The posterior border of the RPE/Bruch's complex is semiautomatically determined (*red line*), while the outer borders of the hyporeflective choriocapillaris (*green line*) and choroid stroma (*blue line*) are manually traced. Plots of mean choroidal thickness (CT) and choriocapillary thickness (CCT) measured from EDI-OCT images of rhesus macaque (**C**) and human eyes (**D**). While CCT is similar between the two species, the measured CT is significantly thinner in macaques than in humans.

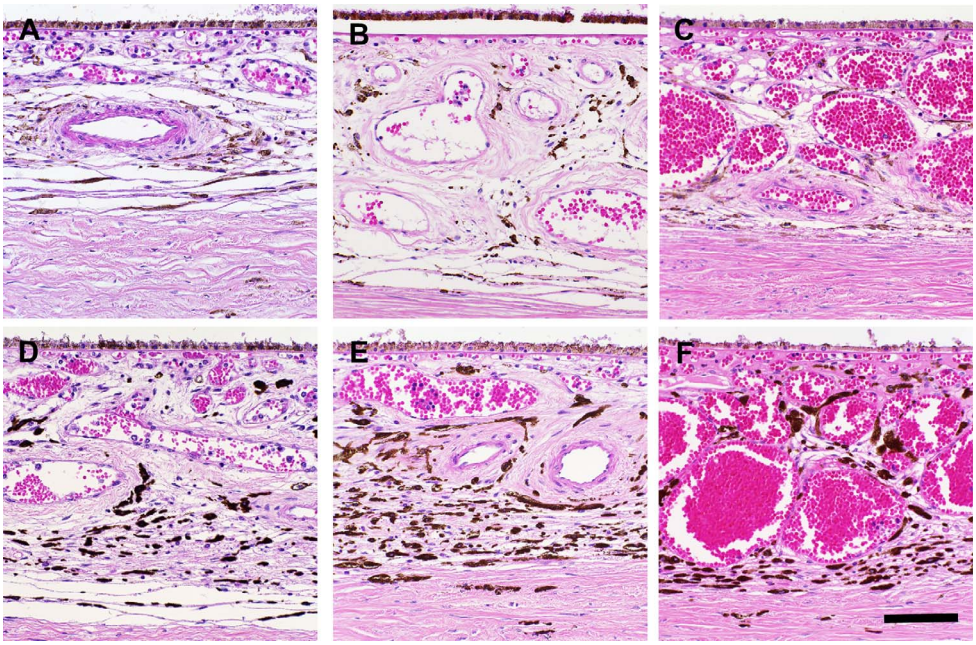

FIGURE 4. Representative histology images of human choroid from white subjects (**A–C**) and black subjects (**D–F**). Histologic sections are taken from (**A**) a 35-year-old white female, (**B**) a 71-year-old white male, (**C**) a 54-year-old white male, (**D**) a 29-year-old black male, (**E**) a 49-year-old black male, and (**F**) a 25-year-old black female.

posteriorly distributed, with the majority of the cells located in Haller's layer and the suprachoroidal layer (Figs. 4A–F).

Consistent with our hypothesis that uveal pigmentation affects choroidal morphology on EDI-OCT, masked grading of images of human eyes showed greater choriocapillaris visibility in black subjects ($P = 0.017$) and higher visibility of the CSJ among white individuals ($P = 0.004$) (Table 4). To determine if race is independently associated with these choroidal morphologic parameters, we performed a multivariate logistic regression including age and refractive error, which are both known determinants of choroidal thickness. Among these factors, our data showed that choriocapillaris visibility was independently associated with race alone ($P = 0.016$), while CSJ visibility was associated with both race ($P = 0.004$) and age ($P = 0.026$) in our study population (Table 5). There were no significant racial differences in both the mean choriocapillary thickness (19.0 ± 3.2 μm in whites vs. 21.0 ± 3.3 μm in blacks; $P = 0.574$) and mean choroidal thickness (240.0 ± 66.2 μm in whites vs. 306.9.8 ± 79.5 μm in blacks; $P = 0.377$). Thus, racial differences have a greater impact on the visibility than the vascular dimensions of the choroid.

DISCUSSION

Together, our results demonstrate that the cross-sectional visualization of choroidal structures including the choriocapillaris and CSJ on EDI-OCT may be affected by pigmented uveal melanocytes in the choroid of humans and rhesus macaques. Additionally, racial differences in pigmentation among human subjects may affect the morphologic appearance of the choroid on EDI-OCT. These results have important implications in human studies, where the ability to define a well-delineated CSJ for reliable choroidal thickness measurements may be affected by the subject's race.

Nonhuman primates are the gold standard among animal models of human macular diseases such as AMD because they possess a macula—a feature absent in most other mammals. Rhesus macaques exhibit AMD-like drusen with a prevalence of up to 50%,[15,16] and even higher in the free-ranging Cayo Santiago colony in Puerto Rico.[22,23] Humans and macaques also share genetic polymorphisms in genes such as *HTRA1* (high temperature requirement factor A1) and *ARMS2* (age-related maculopathy susceptibility 2) that are associated with drusen formation.[24,25] Yet, while OCT imaging has been widely adopted in human clinical practice, the in vivo characterization of the retina and choroid using OCT in rhesus macaques has not been pursued at length. Early work by Toth et al.[26] demonstrated the feasibility of using OCT in primates, while a few later studies employed OCT in macaques to visualize laser-induced choroidal neovascularization.[27,28] The ocular anatomy of rhesus macaques has remarkable resemblance to human eyes, allowing ocular imaging technologies in clinical use to be readily adapted for primate research. As such, our comparative analysis of choroidal morphology in humans and macaques establishes a critical basis for future translational research involving choroidal imaging in these animals.

In this study, we found that the distribution and pigmentation of uveal melanocytes are major determinants of choroidal morphology on EDI-OCT. In macaques, the melanocytes are bigger, more darkly pigmented, and densely dispersed across the choroid stroma up to the posterior border of the choriocapillaris, while in humans they are smaller, less pigmented, and more loosely distributed in the posterior choroid, as described previously.[29] This difference accounts for the more distinctly hyporeflective choriocapillaris band seen in macaques and better delineation of the CSJ in humans on EDI-

TABLE 3. Characteristics of Choroidal Melanocytes in Humans of Different Races

Property	Whites, $n = 18$	Blacks, $n = 12$	P Value
Cell density, cells/10K μm²	31.1 ± 10.3	37.2 ± 15.9	0.49
Average size, μm²/cell	18.3 ± 4.3	38.8 ± 16.8	0.029*
Pigmentation, image luminosity	118.6 ± 27.0	73.4 ± 24.1	0.023*

* Statistical significance ($P < 0.05$) based on Student's t-test.

Table 4. Visibility of Choroidal Morphology in Humans of Different Races

	Choriocapillaris Visibility			Choroidal–Scleral Junction Visibility		
Visibility	Whites, $n = 18$	Blacks, $n = 12$	P Value	Whites, $n = 18$	Blacks, $n = 12$	P Value
<25%	10, 56%	3, 25%	0.017*	5, 28%	10, 84%	0.004*
≥25–<75%	7, 39%	3, 25%		4, 22%	1, 8%	
≥75%	1, 5%	6, 50%		9, 50%	1, 8%	

* Statistical significance ($P < 0.05$) based on Kruskal-Wallis test.

OCT. Interestingly, the retinal layers and RPE appear similar on OCT, and the RPE pigmentation is also similar on histology between the two species. Thus, the melanin pigment in the uvea may be a more important contributor to choroidal morphology on OCT imaging than RPE pigment.

The effect of melanin on OCT reflectivity has been previously addressed. In humans, OCT imaging of patients with ocular albinism shows better visualization of choroidal morphology without EDI due to their reduced pigmentation.[30] Compared to amelanotic nevi, pigmented choroidal nevi on EDI-OCT appear as a highly reflective band with posterior shadowing.[31,32] Patients with choroidal melanocytosis also show an apparent increase in choroidal thickness and perivascular stromal tissue.[33] In animal studies, comparisons of OCT reflectivities from pigmented and albino mice showed differential appearance of the choroid and sclera due to the signal attenuation from choroidal melanin in pigmented mice.[34] Light scattered by tissues containing melanin is also depolarized, as shown in comparisons between pigmented and albino rats, supporting the use of polarization-sensitive OCT technology for imaging pigmented structures in the eye.[35]

We note in our study that race may be an important factor in determining choroidal morphology on EDI-OCT, presumably due to differences in choroidal pigmentation. However, a person's self-identified race is a poor surrogate for pigmentation, and skin color may not correlate well with uveal pigmentation. Other ocular features such as iris color may be a better marker for uveal pigmentation and OCT morphology. Nevertheless, both race and iris color are factors associated with AMD risk,[21,36] and a better understanding of melanin pigmentation in the choroid may provide important insights into the pathophysiology of these retinal diseases. Importantly, the reduced visibility of the CSJ and lower reliability of choroidal thickness measurements in blacks should be taken into account in clinical studies involving multiethnic populations.

The limitations of our study include the small sample size and the retrospective selection of age-matched human subjects for comparative analyses. Many of the normal human eyes were contralateral eyes of subjects with unilateral pathologies that are not known to affect the macular choroid or fellow eye, but an association cannot be completely excluded. Also, the variable appearance of the choriocapillaris in humans may reduce segmentation reliability, while the poor visualization of the CSJ in macaques may lead to an artifactually lower choroidal thickness measurement. Future research using OCT systems such as swept-source OCT devices with longer-wavelength light sources to better visualize deeper ocular structures may help circumvent such limitations.

Table 5. Factors Affecting Choroidal Morphology on EDI-OCT in Humans

	Choriocapillaris Visibility			Choroidal–Scleral Junction Visibility		
Factor	Estimate	SE	P Value	Estimate	SE	P Value
Age	0.002	0.021	0.936	0.061	0.027	0.026*
Refractive error	−0.102	0.244	0.675	−0.036	0.292	0.902
Race†	−2.000	0.832	0.016*	3.221	1.130	0.004*

* Statistical significance ($P < 0.05$).
† Estimate for white race.

While newer technologies such as OCT angiography provide better en face visualization of the choriocapillaris,[37–39] EDI-OCT remains more widely accessible by taking advantage of the existing generation of SD-OCT devices. However, despite some attempts at segmentation of the choriocapillaris or CSJ,[40–43] none have yet to become widely accepted owing to their variable and often ambiguous appearance in human subjects. Our study of choroidal morphology in rhesus macaques showed a very clearly defined choriocapillaris and poor visualization of the CSJ, likely due to the abundance and darker pigmentation of uveal melanocytes in these animals. Future studies on the relationship between melanin pigment and ocular imaging may improve the development of segmentation algorithms and interpretation of OCT findings in retinal and choroidal diseases.

Acknowledgments

The authors thank Alan Proia (Duke University Medical Center) for contributing histologic sections of cadaveric eyes for analysis, and Robert Zawadzki and Chung-Ha Oh for advice on image analyses.

Supported by the California National Primate Research Center Base Grant National Institutes of Health (NIH) P510D011107. GY is supported by the E. Matilda Ziegler Foundation for the Blind, Barr Foundation for Retinal Research, Alcon Research Institute, and NIH K08 EY026101. VV is supported by the National Center for Advancing Translational Sciences and NIH UL1TR000002. SF is supported by NIH P30 EY005722. ST is supported by NIH K08 EY021142. No funding organizations had any role in the design or conduct of this research. The content is solely the responsibility of the authors and does not necessarily represent the official views of the funding agencies.

Disclosure: **G. Yiu**, Alcon (F), Allergan (C, R); **V. S. Vuong**, None; **S. Oltjen**, None; **D. Cunefare**, None; **S. Farsiu**, None; **L. Garzel**, None; **J. Roberts**, None; **S. Thomasy** None

References

1. Nickla DL, Wallman J. The multifunctional choroid. *Prog Retin Eye Res*. 2010;29:144–168.
2. Spaide RF, Koizumi H, Pozzoni MC. Enhanced depth imaging spectral-domain optical coherence tomography. *Am J Ophthalmol*. 2008;146:496–500.
3. Yiu G, Chiu SJ, Petrou PA, et al. Relationship of central choroidal thickness with age-related macular degeneration status. *Am J Ophthalmol*. 2015;159:617–626.e2.
4. Yiu G, Manjunath V, Chiu SJ, Farsiu S, Mahmoud TH. Effect of anti-vascular endothelial growth factor therapy on choroidal thickness in diabetic macular edema. *Am J Ophthalmol*. 2014; 158:745–751.e2.
5. Lin P, Mettu PS, Pomerleau DL, et al. Image inversion spectral-domain optical coherence tomography optimizes choroidal

thickness and detail through improved contrast. *Invest Ophthalmol Vis Sci*. 2012;53:1874–1882.

6. Sanchez-Cano A, Orduna E, Segura F, et al. Choroidal thickness and volume in healthy young white adults and the relationships between them and axial length, ammetropy and sex. *Am J Ophthalmol*. 2014;158:574–583.e1.
7. Spaide RF. Age-related choroidal atrophy. *Am J Ophthalmol*. 2009;147:801–810.
8. Maruko I, Iida T, Sugano Y, Ojima A, Ogasawara M, Spaide RF. Subfoveal choroidal thickness after treatment of central serous chorioretinopathy. *Ophthalmology*. 2010;117:1792–1799.
9. Jirarattanasopa P, Ooto S, Tsujikawa A, et al. Assessment of macular choroidal thickness by optical coherence tomography and angiographic changes in central serous chorioretinopathy. *Ophthalmology*. 2012;119:1666–1678.
10. da Silva FT, Sakata VM, Nakashima A, et al. Enhanced depth imaging optical coherence tomography in long-standing Vogt-Koyanagi-Harada disease. *Br J Ophthalmol*. 2013;97:70–74.
11. Maruko I, Iida T, Sugano Y, et al. Subfoveal choroidal thickness after treatment of Vogt-Koyanagi-Harada disease. *Retina*. 2011; 31:510–517.
12. Nakayama M, Keino H, Okada AA, et al. Enhanced depth imaging optical coherence tomography of the choroid in Vogt-Koyanagi-Harada disease. *Retina*. 2012;32:2061–2069.
13. Adhi M, Brewer E, Waheed NK, Duker JS. Analysis of morphological features and vascular layers of choroid in diabetic retinopathy using spectral-domain optical coherence tomography. *JAMA Ophthalmol*. 2013;131:1267–1274.
14. Adhi M, Lau M, Liang MC, Waheed NK, Duker JS. Analysis of the thickness and vascular layers of the choroid in eyes with geographic atrophy using spectral-domain optical coherence tomography. *Retina*. 2014;34:306–312.
15. Bellhorn RW, King CD, Aguirre GD, Ripps H, Siegel IM, Tsai HC. Pigmentary abnormalities of the macula in rhesus monkeys: clinical observations. *Invest Ophthalmol Vis Sci*. 1981;21:771–781.
16. Stafford TJ, Anness SH, Fine BS. Spontaneous degenerative maculopathy in the monkey. *Ophthalmology*. 1984;91:513–521.
17. Chiu SJ, Li XT, Nicholas P, Toth CA, Izatt JA, Farsiu S. Automatic segmentation of seven retinal layers in SDOCT images congruent with expert manual segmentation. *Opt Express*. 2010;18:19413–19428.
18. Vuong VS, Moisseiev E, Cunefare D, Farsiu S, Moshiri A, Yiu G. Repeatability of choroidal thickness measurements on enhanced depth imaging OCT using different posterior boundaries. *Am J Ophthalmol*. 2016;169:104–112.
19. Bland JM, Altman DG. Statistical methods for assessing agreement between two methods of clinical measurement. *Lancet*. 1986;1:307–310.
20. Yiu G, Pecen P, Sarin N, et al. Characterization of the choroid-scleral junction and suprachoroidal layer in healthy individuals on enhanced-depth imaging optical coherence tomography. *JAMA Ophthalmol*. 2014;132:174–181.
21. Weiter JJ, Delori FC, Wing GL, Fitch KA. Retinal pigment epithelial lipofuscin and melanin and choroidal melanin in human eyes. *Invest Ophthalmol Vis Sci*. 1986;27:145–152.
22. Hope GM, Dawson WW, Engel HM, Ulshafer RJ, Kessler MJ, Sherwood MB. A primate model for age related macular drusen. *Br J Ophthalmol*. 1992;76:11–16.
23. El-Mofty A, Gouras P, Eisner G, Balazs EA. Macular degeneration in rhesus monkey (Macaca mulatta). *Exp Eye Res*. 1978; 27:499–502.
24. Francis PJ, Appukuttan B, Simmons E, et al. Rhesus monkeys and humans share common susceptibility genes for age-related macular disease. *Hum Mol Genet*. 2008;17:2673–2680.
25. Singh KK, Krawczak M, Dawson WW, Schmidtke J. Association of HTRA1 and ARMS2 gene variation with drusen formation in rhesus macaques. *Exp Eye Res*. 2009;88:479–482.
26. Toth CA, Narayan DG, Boppart SA, et al. A comparison of retinal morphology viewed by optical coherence tomography and by light microscopy. *Arch Ophthalmol*. 1997;115:1425–1428.
27. Wang Q, Lin X, Xiang W, Xiao W, He M. Assessment of laser induction of Bruch's membrane disruption in monkey by spectral-domain optical coherence tomography. *Br J Ophthalmol*. 2015;99:119–124.
28. Fukuchi T, Takahashi K, Uyama M, Matsumura M. Comparative study of experimental choroidal neovascularization by optical coherence tomography and histopathology. *Jpn J Ophthalmol*. 2001;45:252–258.
29. Krebs W, Krebs I. Primate Retina and Choroid: Atlas of Fine Structure in Man and Monkey. New York: Springer-Verlag; 1991.
30. Chong GT, Farsiu S, Freedman SF, et al. Abnormal foveal morphology in ocular albinism imaged with spectral-domain optical coherence tomography. *Arch Ophthalmol*. 2009;127: 37–44.
31. Torres VL, Brugnoni N, Kaiser PK, Singh AD. Optical coherence tomography enhanced depth imaging of choroidal tumors. *Am J Ophthalmol*. 2011;151:586–593.e2.
32. Shah SU, Kaliki S, Shields CL, Ferenczy SR, Harmon SA, Shields JA. Enhanced depth imaging optical coherence tomography of choroidal nevus in 104 cases. *Ophthalmology*. 2012;119: 1066–1072.
33. Pellegrini M, Shields CL, Arepalli S, Shields JA. Choroidal melanocytosis evaluation with enhanced depth imaging optical coherence tomography. *Ophthalmology*. 2014;121: 257–261.
34. Zhang P, Goswami M, Zawadzki RJ, Pugh EN Jr. The photosensitivity of rhodopsin bleaching and light-induced increases of fundus reflectance in mice measured in vivo with scanning laser ophthalmoscopy. *Invest Ophthalmol Vis Sci*. 2016;57:3650–3664.
35. Baumann B, Schirmer J, Rauscher S, et al. Melanin pigmentation in rat eyes: in vivo imaging by polarization-sensitive optical coherence tomography and comparison to histology. *Invest Ophthalmol Vis Sci*. 2015;56:7462–7472.
36. Frank RN, Puklin JE, Stock C, Canter LA. Race, iris color, and age-related macular degeneration. *Trans Am Ophthalmol Soc*. 2000;98:109–115, discussion 115–117.
37. Choi W, Moult EM, Waheed NK, et al. Ultrahigh-speed swept-source optical coherence tomography angiography in non-exudative age-related macular degeneration with geographic atrophy. *Ophthalmology*. 2015;122:2532–2544.
38. Waheed NK, Moult EM, Fujimoto JG, Rosenfeld PJ. Optical coherence tomography angiography of dry age-related macular degeneration. *Dev Ophthalmol*. 2016;56:91–100.
39. Kim DY, Fingler J, Zawadzki RJ, et al. Optical imaging of the chorioretinal vasculature in the living human eye. *Proc Natl Acad Sci U S A*. 2013;110:14354–14359.
40. Branchini LA, Adhi M, Regatieri CV, et al. Analysis of choroidal morphologic features and vasculature in healthy eyes using spectral-domain optical coherence tomography. *Ophthalmology*. 2013;120:1901–1908.
41. Almeida DR, Zhang L, Chin EK, et al. Comparison of retinal and choriocapillaris thicknesses following sitting to supine transition in healthy individuals and patients with age-related macular degeneration. *JAMA Ophthalmol*. 2015;133:297–303.
42. Zhang L, Lee K, Niemeijer M, Mullins RF, Sonka M, Abramoff MD. Automated segmentation of the choroid from clinical SD-OCT. *Invest Ophthalmol Vis Sci*. 2012;53:7510–7519.
43. Invernizzi A, Agarwal A, Cozzi M, Viola F, Nguyen QD, Staurenghi G. Enhanced depth imaging optical coherence tomography features in areas of choriocapillaris hypoperfusion. *Retina*. 2016;36:2013–2021.

Investigative Ophthalmology & Visual Science